

# Vector magnetic field sensing via multi-frequency control of nitrogen-vacancy centers in diamond

Sayaka Kitazawa,<sup>1</sup> Yuichiro Matsuzaki,<sup>2</sup> Saijo Soya,<sup>3</sup> Kosuke Kakuyanagi,<sup>2</sup> Shiro Saito,<sup>2</sup> and Junko Ishi-Hayase<sup>3</sup>

<sup>1</sup> *Department of Applied Physics and Department of Physico-Informatics, Faculty of Science and Technology, Keio University, Hiyoshi, Kohoku-ku, Yokohama 223-8522, Japan*

<sup>2</sup> *NTT Basic Research Laboratories, NTT Corporation, 3-1 Morinosato-Wakamiya, Atsugi, Kanagawa, 243-0198, Japan.*

<sup>3</sup> *Department of Applied Physics and Department of Physico-Informatics, Faculty of Science and Technology, Keio University, Hiyoshi, Kohoku-ku, Yokohama 223-8522, Japan*

An ensemble of nitrogen-vacancy (NV) centers in diamond is an attractive device to detect small magnetic fields. In particular, by exploiting the fact that the NV center can be aligned along one of four different axes due to  $C_{3v}$  symmetry, it is possible to extract information concerning vector magnetic fields. However, in the conventional scheme, low readout contrasts of the NV centers significantly decrease the sensitivity of the vector magnetic field sensing. Here, we propose a way to improve the sensitivity of the vector magnetic field sensing of the NV centers using multi-frequency control. Since the Zeeman energy of the NV centers depends on the direction of the axis, we can independently control the four types of NV centers using microwave pulses with different frequencies. This allows us to use every NV center for the vector field detection in parallel, which effectively increases the readout contrast. Our results pave the way to realize a practical diamond-based vector field sensor.

The detection of small magnetic fields is important in the field of metrology, because there are many potential applications in biology and medical science. The performance of a magnetic field sensor is characterized by its spatial resolution and sensitivity; therefore, a significant amount of effort has been devoted to creating a device that can measure small magnetic fields in a local region [1–3].

Nitrogen vacancy (NV) centers in diamond are fascinating candidates with which to construct a magnetic field sensor [4–7]. The NV center is a spin 1 system, and the frequency of the  $|\pm 1\rangle$  states can be shifted by magnetic fields. We can use this system as an effective two-level system spanned by  $|0\rangle$  and  $|1\rangle$  with a frequency selectivity where  $|-1\rangle$  is significantly detuned. We can implement gate operations of the spins in NV centers using microwave pulses [8–11]. It is possible to detect DC (AC) magnetic fields by implementing a Ramsey interference (spin echo) measurement [4–6]. Moreover, NV centers have a long coherence time, e.g., a few milli-seconds at a room temperature and a second at low temperature [12–14]. In addition, because the NV centers can be strongly coupled with optical photons, we can read out the state of the NV centers via fluorescence from the optical transitions [9, 10]. The NV centers can be embedded in nanocrystals, which allows the NV centers to interact with local magnetic fields [15]. These properties are prerequisite to realizing a high-performance sensor for magnetic fields.

Recently, vector magnetic field sensing by NV centers has become an active area of interest [16–21]. The NV center is aligned along one of four different axes due to  $C_{3v}$  symmetry. The Zeeman energies of the NV centers are determined by  $g\mu_b\mathbf{B} \cdot \mathbf{d}_j$  ( $j = 1, 2, 3, 4$ ) where  $g$  denotes the g factor,  $\mu_b$  denotes a Bohr magneton,  $\mathbf{B}$  denotes the magnetic fields, and  $\mathbf{d}_j$  denotes the direction of the  $j$ -th NV axis. By sequentially performing Ramsey interference or spin echo measurements on NV centers with different NV axes, we can estimate the values of the Zeeman energies  $g\mu_b\mathbf{B} \cdot \mathbf{d}_j$ . The data from the experiments can be processed to reconstruct the vector com-

ponents ( $B_x$ ,  $B_y$ , and  $B_z$ ) of applied magnetic fields [16, 18]. This can be used to magnetically image a target sample such as living cells or circuit currents [22, 23].

In the conventional approach, the low readout contrast of the NV centers decreases the sensitivity when sensing the vector magnetic field [5, 24]. When the state of the NV centers is  $|\pm 1\rangle$ , the photoluminescence intensity becomes smaller than in the case of  $|0\rangle$ . This allows us to measure the state of the NV centers via optical detection even at room temperature. Nevertheless, we can only detect a small portion of the emitted photons, because most of the photons are emitted into the environment. This decreases the readout contrast. Moreover, if we only implement Ramsey or spin echo measurements on NV centers with a specific axis with this limited readout contrast, the states of the other NV centers with different axes remain in the  $|0\rangle$  state regardless the value of the magnetic fields, which induces noise affecting the sensitivity of the magnetic field sensor [5]. If we only need to estimate one vector component of the target magnetic field, we can recover the sensitivity by using a diamond where the orientations of the NV centers are aligned along just one axis [25–27]. However, we cannot use such a diamond to estimate every component of the vector magnetic fields, unless we mechanically rotate the diamond to change the angle between the target magnetic fields and the direction of the NV axis.

Here, we propose a scheme to improve the sensitivity of the vector magnetic field sensing via multi-frequency control. Because NV centers with different axes can have different resonant frequencies [24], we can independently control these NV centers via frequency selectivity. The key idea in our scheme is the simultaneous implementation of a Ramsey interference or spin echo experiment with every NV center by via multi-frequency control. We show that adequate control of the microwave pulses can enhance the signal from NV centers with four different axes, and that the sensitivity of the vector magnetic field sensing becomes approximately four times better than that of the conventional scheme.

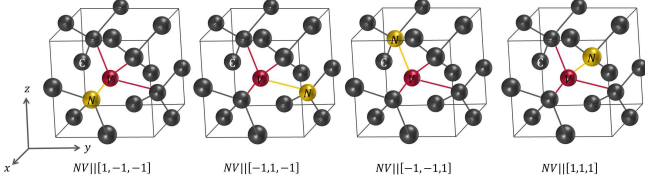


FIG. 1: An NV center in diamond set an axis to be the direction from the vacancy to the nitrogen. There are four possible directions of the axis in the diamond. Note that, by applying known external magnetic fields, we can independently control the four types of NV centers with different axes using frequency selectivity.

### CONVENTIONAL VECTOR MAGNETIC FIELD SENSING WITH AN NV CENTER

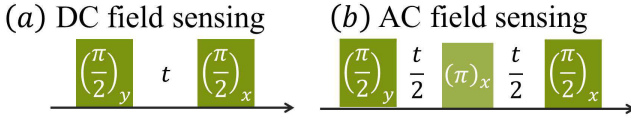


FIG. 2: Microwave pulse sequence for standard magnetometry with NV centers; (a) Ramsey interference measurements performed to sense DC field, and (b) Spin echo measurements performed to sense the AC field where we can suppress low frequency magnetic field noise.

Here, we review conventional DC magnetic field sensing using NV centers [5, 16, 17]. Even though the NV center is a spin-1 system, we can treat it as a two-level system spanned by  $|0\rangle$  and  $|1\rangle$  with frequency selectivity. Note that the NV center has four types of intrinsic quantization axes along the NV direction with zero or small magnetic fields. We define the direction of these NV axes as  $\mathbf{d}_1 = (\frac{1}{\sqrt{3}}, -\frac{1}{\sqrt{3}}, -\frac{1}{\sqrt{3}})$ ,  $\mathbf{d}_2 = (-\frac{1}{\sqrt{3}}, \frac{1}{\sqrt{3}}, -\frac{1}{\sqrt{3}})$ ,  $\mathbf{d}_3 = (-\frac{1}{\sqrt{3}}, -\frac{1}{\sqrt{3}}, \frac{1}{\sqrt{3}})$ , and  $\mathbf{d}_4 = (\frac{1}{\sqrt{3}}, \frac{1}{\sqrt{3}}, \frac{1}{\sqrt{3}})$ . The Hamiltonian of the NV center with an axis defined by a vector  $\mathbf{d}_k$  is given as

$$H_k = \frac{\omega_k}{2} \hat{\sigma}_z + \lambda \hat{\sigma}_x \cos \omega'_k t \quad (1)$$

where  $\omega_k = \omega_0 + g\mu_b \mathbf{B}_{\text{total}} \cdot \mathbf{d}_k$ ,  $\omega_0$  denotes a zero field splitting,  $g\mu_b \mathbf{B}_{\text{total}} \cdot \mathbf{d}_k$  denotes a Zeeman energy splitting,  $\mathbf{B}_{\text{total}} = \mathbf{B}_{\text{ex}} + \mathbf{B}$  denotes the sum of a known external magnetic field ( $\mathbf{B}_{\text{ex}}$ ) and the target unknown magnetic field ( $\mathbf{B}$ ),  $\lambda$  denotes a Rabi frequency, and  $\omega'_k$  denotes a microwave frequency. In a rotating frame, we can rewrite this Hamiltonian as

$$H_k = \frac{\omega_k - \omega'_k}{2} \hat{\sigma}_z + \frac{\lambda}{2} \hat{\sigma}_x \quad (2)$$

where we choose  $\omega'_k = \omega_0 + g\mu_b \mathbf{B}_{\text{ex}} \cdot \mathbf{d}_k$ . If we do not apply a microwave, the Hamiltonian in the rotating frame is written as

$$H_k = \frac{g\mu_b \mathbf{B} \cdot \mathbf{d}_k}{2} \hat{\sigma}_z \quad (3)$$

We can construct the vector field sensor as follows (see Fig. 2(a)). We assume that the initialization time, pulse operations, and readout time are much shorter than the coherence time of the NV center. First, we initialize  $|0\rangle_k$  state via green laser irradiation. Second, by performing a  $\frac{\pi}{2}$  pulse along the  $y$  axis with the microwave, we prepare a  $|+\rangle_k = \frac{1}{\sqrt{2}}(|0\rangle_k + |1\rangle_k)$  state. Third, we let this state evolve via the Hamiltonian in Eq. (2) for a time  $t_k$ . Note that the NV center is affected by the dephasing process; therefore, the dynamics can be described by the following master equation.

$$\frac{d\rho_k}{dt} = -i[H_k, \rho_k] - \gamma_k(\rho_k - \hat{\sigma}_z \rho_k \hat{\sigma}_z) \quad (4)$$

where  $\gamma_k = \frac{1}{2T_2^{k*}}$  denotes the dephasing rate of the  $k$  the NV center and  $T_2^{k*}$  denotes the coherence time measured by Ramsey interference. Fourth, we perform a  $\frac{\pi}{2}$  pulse along the  $x$  axis with the microwave. The diagonal component of the density matrix after these operations can be calculated to be

$${}_k \langle 0 | \rho_k(t_k) | 0 \rangle_k = \frac{1 + e^{-2\gamma_k t_k} \sin(g\mu_b \mathbf{B} \cdot \mathbf{d}_k t_k)}{2} \quad (5)$$

$${}_k \langle 1 | \rho_k(t_k) | 1 \rangle_k = \frac{1 - e^{-2\gamma_k t_k} \sin(g\mu_b \mathbf{B} \cdot \mathbf{d}_k t_k)}{2}. \quad (6)$$

Finally, we readout the population of the state via the green laser irradiation [9]. The information of the NV center is now transferred into photons, and the photon state is described as

$$\begin{aligned} \rho_k^{(\text{ph})} &= \frac{1 + e^{-2\gamma_k t_k} \sin(g\mu_b \mathbf{B} \cdot \mathbf{d}_k t_k)}{2} \rho_{k,0}^{(\text{ph})} \\ &+ \frac{1 - e^{-2\gamma_k t_k} \sin(g\mu_b \mathbf{B} \cdot \mathbf{d}_k t_k)}{2} \rho_{k,1}^{(\text{ph})} \end{aligned} \quad (7)$$

where  $\rho_{k,1}^{(\text{ph})}$  ( $\rho_{k,0}^{(\text{ph})}$ ) denotes the state of the photon after performing the green laser pulse when the state of the NV center is  $|0\rangle_k$  ( $|1\rangle_k$ ). We can describe  $\rho_{k,1}^{(\text{ph})}$  and  $\rho_{k,0}^{(\text{ph})}$  as follows.

$$\begin{aligned} \rho_{k,0}^{(\text{ph})} &= (1 - \tilde{\alpha}_0^{(k)}) |0\rangle_{\text{ph}} \langle 0| + \tilde{\alpha}_0^{(k)} |1\rangle_{\text{ph}} \langle 1| \\ \rho_{k,1}^{(\text{ph})} &= (1 - \tilde{\alpha}_1^{(k)}) |0\rangle_{\text{ph}} \langle 0| + \tilde{\alpha}_1^{(k)} |1\rangle_{\text{ph}} \langle 1| \end{aligned}$$

where  $|0\rangle_{\text{ph}}$  and  $|1\rangle_{\text{ph}}$  denote the Fock states of the photon. We define

$$\begin{aligned} \tilde{\alpha}_0^{(k)} &= \sum_{j=1}^4 \alpha_0^{(j)} \\ \tilde{\alpha}_1^{(k)} &= \alpha_1^{(k)} + \sum_{j \neq k} \alpha_0^{(j)} \end{aligned} \quad (8)$$

where  $\alpha_0^{(k)}$  ( $\alpha_1^{(k)}$ ) for  $k = 1, 2, 3, 4$  denotes the probability emitting a photon when the state of the NV center is  $|0\rangle_k$  ( $|1\rangle_k$ ). Note that, while we control the NV center with the NV axis along  $\mathbf{d}_k$ , the other NV centers remain the  $|0\rangle$  state and emit photons. We assume  $\alpha_0^{(k)}, \alpha_1^{(k)} \ll 1$  and that the

multiple photon emission probability from an NV center is negligible. For  $g\mu_b \mathbf{B} \cdot \mathbf{d}_k t_k \ll 1$ , we can calculate the expectation value of the emitted photons

$$\begin{aligned} \langle \hat{N}_k \rangle &= \text{Tr}[\rho_k^{(\text{ph})} \hat{N}] \\ &\simeq \frac{1 + g\mu_b \mathbf{B} \cdot \mathbf{d}_k t_k e^{-2\gamma_k t_k}}{2} \tilde{\alpha}_0^{(k)} \\ &+ \frac{1 - g\mu_b \mathbf{B} \cdot \mathbf{d}_k t_k e^{-2\gamma_k t_k}}{2} \tilde{\alpha}_1^{(k)} \end{aligned} \quad (9)$$

where  $\hat{N} = \sum_{n=0}^{\infty} |n\rangle_{\text{ph}} \langle n|$ . Note that we can tune  $\alpha_0^{(k)}$  and  $\alpha_1^{(k)}$  by changing both the applied known magnetic fields and the polarization of the photons. In addition, we can decrease the coherence time if we add artificial noise. For simplicity, we assume  $\alpha_0^{(k)} = \alpha_0$ ,  $\alpha_1^{(k)} = \alpha_1$ ,  $\gamma_k = \gamma$ , and  $t_k = t$  for all  $k$ . Suppose we first implement the above experiment shown in Fig. 2(a) for  $k = 1$ , and then implement it for  $k = 4$ , which allows us to sum up these two experimental data. We obtain

$$\begin{aligned} &\langle \hat{N}_1 \rangle + \langle \hat{N}_4 \rangle \\ &= (\tilde{\alpha}_0 + \tilde{\alpha}_1) + \frac{1}{\sqrt{3}} (\tilde{\alpha}_0 - \tilde{\alpha}_1) g\mu_b B_x t e^{-2\gamma t} \end{aligned} \quad (10)$$

Interestingly, this sum depends on  $B_x$  while this is independent of  $B_y$  and  $B_z$ . Therefore we define  $\langle \hat{N}_x \rangle \equiv \langle \hat{N}_1 \rangle + \langle \hat{N}_4 \rangle$ , and we estimate  $B_x$  from  $\langle \hat{N}_x \rangle$ . Note that, even though we explain the case to measure  $B_x$ , we can also measure  $B_y$  ( $B_z$ ) by considering  $\langle \hat{N}_y \rangle \equiv \langle \hat{N}_2 \rangle + \langle \hat{N}_4 \rangle$  ( $\langle \hat{N}_z \rangle \equiv \langle \hat{N}_3 \rangle + \langle \hat{N}_4 \rangle$ ), because  $\langle \hat{N}_y \rangle$  ( $\langle \hat{N}_z \rangle$ ) only depends on  $B_y$  ( $B_z$ ). Therefore, we can calculate the uncertainty in the estimation of  $B_x$  as follows.

$$\begin{aligned} \delta B_x^{(\text{DC})} &= \frac{\sqrt{\langle \delta \hat{N}_x \delta \hat{N}_x \rangle}}{\left| \frac{d\langle \hat{N}_x \rangle}{dB_x} \right|} \frac{1}{\sqrt{N}} \\ &= \frac{\sqrt{3}\sqrt{7\alpha_0 + \alpha_1}}{|\alpha_0 - \alpha_1| g\mu_b t e^{-2\gamma t}} \frac{1}{\sqrt{\frac{T}{2t}}} \end{aligned} \quad (11)$$

where  $N = \frac{T}{2t}$  denotes the repetition number and  $T$  denotes the total experiment time. This uncertainty is minimized for  $t = \frac{1}{4\gamma}$  and,

$$\delta B_x^{(\text{DC})} = \frac{\sqrt{3}\sqrt{7\alpha_0 + \alpha_1}}{e^{-\frac{1}{4}} |\alpha_0 - \alpha_1| g\mu_b \sqrt{\frac{1}{4\gamma}}} \frac{1}{\sqrt{\frac{T}{2}}} \quad (12)$$

Therefore we chose this value for the field sensing. Note that we have a factor of  $\sqrt{7\alpha_0 + \alpha_1}$  in the numerator, which increases the uncertainty. This is because, when we readout the NV centers, three quarters of the NV centers remain in the  $|0\rangle$  state regardless of strength of the magnetic fields, which decreases the sensitivity. This clearly shows that the existence of NV centers that emit the same amount of photons regardless of the strength of the applied magnetic field actually decreases the sensitivity of the field sensing.

Here, we briefly review conventional AC magnetic field sensing using NV centers [5, 16, 17]. We have the same form of the Hamiltonian described in Eq. 1 where we replace the total magnetic field with  $\mathbf{B}_{\text{total}} = \mathbf{B}_{\text{ex}} + \mathbf{B}_{\text{AC}} \sin \omega_{\text{AC}} t$ . To estimate the values of  $\mathbf{B}_{\text{AC}}$ , we use a similar pulse sequence to that of the DC magnetic field sensing. The only difference from the DC magnetic field sensing is that we apply a  $\pi$  pulse in the middle of the time evolution between the two  $\frac{\pi}{2}$  pulse, as shown in Fig. 2 (b). The diagonal component of the density matrix can be calculated as

$${}_k \langle 0 | \rho_k(t_k) | 0 \rangle_k = \frac{1 + e^{-2\gamma'_k t_k} \sin \theta_k^{(\text{AC})}}{2} \quad (13)$$

$${}_k \langle 1 | \rho_k(t_k) | 1 \rangle_k = \frac{1 - e^{-2\gamma'_k t_k} \sin \theta_k^{(\text{AC})}}{2}. \quad (14)$$

$$\theta_k^{(\text{AC})} = g\mu_b \mathbf{B} \cdot \mathbf{d}_k \frac{1 + \cos \omega_{\text{AC}} t - 2 \cos \frac{\omega_{\text{AC}} t}{2}}{\omega_{\text{AC}}} \quad (15)$$

where  $\gamma'_k = \frac{1}{2T_2^k}$  denotes the dephasing rate for the  $k'$  th NV center and  $T_2^k$  denotes the dephasing time measured by the spin echo. Similar to the case of DC sensing, we can calculate the sensitivity of the AC field sensing such that

$$\delta B_x^{(\text{AC})} \simeq \frac{\sqrt{3}\sqrt{7\alpha_0 + \alpha_1}}{|\alpha_0 - \alpha_1| g\mu_b \frac{|1 + \cos \omega_{\text{AC}} t - 2 \cos \frac{\omega_{\text{AC}} t}{2}|}{\omega_{\text{AC}}} e^{-2\gamma' t}} \frac{1}{\sqrt{\frac{T}{2t}}} \quad (16)$$

where we assume  $\alpha_0^{(k)} = \alpha_0$ ,  $\alpha_1^{(k)} = \alpha_1$ ,  $\gamma'_k = \gamma'$ , and  $t_k = t$  for all  $k$ . This uncertainty is minimized for  $t = \frac{1}{4\gamma'}$  and  $\omega_{\text{AC}} \simeq 23.3\gamma' = \frac{2\theta_{\text{opt}}}{T_2}$  for  $\theta_{\text{opt}} \simeq 1.856\pi$ ; therefore, we choose these values for the field sensing. The uncertainty in the estimation is given as follows.

$$\delta B_x^{(\text{AC})} \simeq \frac{\sqrt{3}\sqrt{7\alpha_0 + \alpha_1}}{e^{-\frac{1}{2}} |\alpha_0 - \alpha_1| g\mu_b \frac{|1 + \cos \theta_{\text{opt}} - 2 \cos \frac{\theta_{\text{opt}}}{2}|}{\theta_{\text{opt}}} \sqrt{\frac{1}{4\gamma'}}} \frac{1}{\sqrt{\frac{T}{2}}} \quad (17)$$

## DC VECTOR MAGNETIC FIELD SENSOR VIA MULTI-FREQUENCY CONTROL

Here, we propose a scheme to measure the vector magnetic field with an improved sensitivity. The key idea is to adopt multi-frequency control of the NV centers. NV centers with different axes can have different resonant frequencies when applying a known external magnetic field [24]; therefore, we can independently control these NV centers using frequency selectivity. In addition, we can parallelize the control of the NV centers by simultaneously rotating all NV centers with different axes so that every NV center can be involved in the field sensing.

As an example, we explain how to measure a DC magnetic field component along  $[1, 0, 0]$  ( $B_x$ ) using our scheme. After the initialization of the states by the green laser, we rotate every NV center using the  $\frac{\pi}{2}$  pulse, and the initial state is given

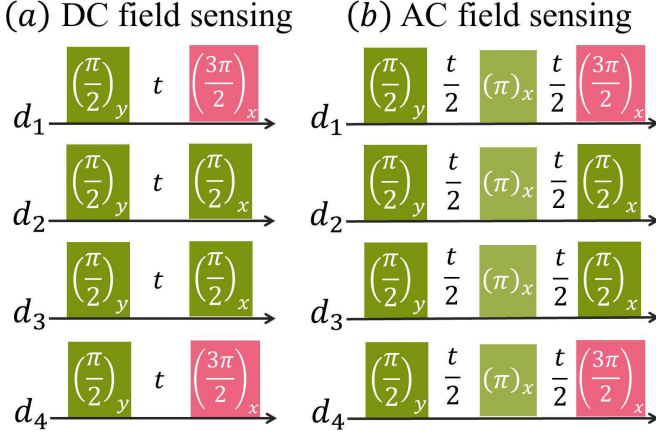


FIG. 3: The pulse sequence used to perform our proposed vector magnetic field sensing. Using frequency selectivity, we independently control the NV centers with different axes. We implement four microwave pulses with different frequencies at the same time to increase the sensitivity.

by

$$\bigotimes_{k=1}^4 \frac{1}{\sqrt{2}} (|0\rangle_k + |1\rangle_k). \quad (18)$$

We let this state evolve for a time  $t$  according to the master equation in Eq. (4). After performing the  $\frac{\pi}{2}$  pulse ( $\frac{3\pi}{2}$  pulse) on the NV centers with the NV axes  $\mathbf{d}_2$  and  $\mathbf{d}_3$  ( $\mathbf{d}_1$  and  $\mathbf{d}_4$ ) as shown in Fig. 3(a), we read out the state of the NV centers via the photoluminescence. The diagonal component of the density matrix just before the readout can be calculated to be

$$\begin{aligned} {}_k \langle 0 | \rho_k(t_k) | 0 \rangle_k &= \frac{1 + e^{-2\gamma_k t_k} \sin(g\mu_b \mathbf{B} \cdot \mathbf{d}_k t_k)}{2} \\ {}_k \langle 1 | \rho_k(t_k) | 1 \rangle_k &= \frac{1 - e^{-2\gamma_k t_k} \sin(g\mu_b \mathbf{B} \cdot \mathbf{d}_k t_k)}{2} \end{aligned} \quad (19)$$

for  $k = 2, 3$  and

$$\begin{aligned} {}_k \langle 0 | \rho_k(t_k) | 0 \rangle_k &= \frac{1 - e^{-2\gamma_k t_k} \sin(g\mu_b \mathbf{B} \cdot \mathbf{d}_k t_k)}{2} \\ {}_{k'} \langle 1 | \rho_k(t_k) | 1 \rangle_k &= \frac{1 + e^{-2\gamma_k t_k} \sin(g\mu_b \mathbf{B} \cdot \mathbf{d}_k t_k)}{2} \end{aligned} \quad (20)$$

for  $k = 1, 4$ . After the green laser irradiation, the state of the photons can be described as follows.

$$\rho^{(\text{ph})} = \bigotimes_{k=1}^4 \rho_k^{(\text{ph})} \quad (21)$$

where

$$\begin{aligned} \rho_k^{(\text{ph})} &= \frac{1 + e^{-2\gamma_k t_k} \sin(g\mu_b \mathbf{B} \cdot \mathbf{d}_k t_k)}{2} \rho_{k,0}^{(\text{ph})} \\ &+ \frac{1 - e^{-2\gamma_k t_k} \sin(g\mu_b \mathbf{B} \cdot \mathbf{d}_k t_k)}{2} \rho_{k,1}^{(\text{ph})} \end{aligned} \quad (22)$$

for  $k = 2, 3$  and

$$\begin{aligned} \rho_k^{(\text{ph})} &= \frac{1 - e^{-2\gamma_k t_k} \sin(g\mu_b \mathbf{B} \cdot \mathbf{d}_k t_k)}{2} \rho_{k,0}^{(\text{ph})} \\ &+ \frac{1 + e^{-2\gamma_k t_k} \sin(g\mu_b \mathbf{B} \cdot \mathbf{d}_k t_k)}{2} \rho_{k,1}^{(\text{ph})} \end{aligned} \quad (23)$$

for  $k = 1, 4$ . We can calculate the expected values of the emitted photons from these states as follows:

$$\begin{aligned} \langle \hat{N}_x^{(\text{total})} \rangle &= \text{Tr} \left[ \left( \sum_{k=1}^4 \hat{N}_k \right) \rho^{(\text{ph})} \right] \\ &\simeq \sum_{k=1}^4 \frac{\alpha_0^{(k)} + \alpha_1^{(k)}}{2} \\ &- \sum_{k=1,4} \frac{\alpha_0^{(k)} - \alpha_1^{(k)}}{2} g\mu_b \mathbf{B} \cdot \mathbf{d}_k t_k e^{-2\gamma_k t_k} \\ &+ \sum_{k=2,3} \frac{\alpha_0^{(k)} - \alpha_1^{(k)}}{2} g\mu_b \mathbf{B} \cdot \mathbf{d}_k t_k e^{-2\gamma_k t_k} \end{aligned} \quad (24)$$

If we have  $\alpha_0^{(k)} = \alpha_0$ ,  $\alpha_1^{(k)} = \alpha_1$ ,  $\gamma_k = \gamma$ , and  $t_k = t$  for all  $k$ , we obtain

$$\langle \hat{N}_x^{(\text{total})} \rangle \simeq 2(\alpha_0 + \alpha_1) - \frac{2}{\sqrt{3}} (\alpha_0 - \alpha_1) g\mu_b B_x t e^{-2\gamma t}$$

Note that this expectation values depends on just  $B_x$ . Therefore, the uncertainty of the estimation of  $B_x$  is given as follows.

$$\begin{aligned} \delta B_x^{(\text{DC})} &= \frac{\sqrt{\langle \delta \hat{N}_x^{(\text{total})} \delta \hat{N}_x^{(\text{total})} \rangle}}{\left| \frac{d \langle \hat{N}_x^{(\text{total})} \rangle}{dB_x} \right|} \frac{1}{\sqrt{N}} \\ &\simeq \frac{\sqrt{2(\alpha_0 + \alpha_1)}}{\frac{2}{\sqrt{3}} |\alpha_0 - \alpha_1| g\mu_b t e^{-2\gamma t}} \frac{1}{\sqrt{\frac{T}{t}}} \end{aligned} \quad (25)$$

where  $N = \frac{T}{t}$  denotes the repetition number of the experiment. This uncertainty is minimized for  $t = \frac{1}{4\gamma}$  and

$$\delta B_x^{(\text{DC})} \simeq \frac{\sqrt{3} \sqrt{2(\alpha_0 + \alpha_1)}}{2e^{-\frac{1}{2}} |\alpha_0 - \alpha_1| g\mu_b \sqrt{\frac{1}{4\gamma}}} \frac{1}{\sqrt{T}} \quad (26)$$

Therefore, we chose this value for the field sensing. Because we have  $\alpha_0 \simeq \alpha_1$  due to the low readout contrast [24], the sensitivity of our scheme described by (Eq. 26) is approximately four times better than that in the conventional scheme described by Eq. (12). Note that, even though we explained how to measure the magnetic field  $B_x$  along  $[1, 0, 0]$ , we can easily generalize our scheme to measure  $B_y$  and  $B_z$ . For example, to measure  $B_y$  ( $B_z$ ), we perform a  $\frac{\pi}{2}$  pulse ( $\frac{3\pi}{2}$  pulse) on the NV centers with the NV axes of  $\mathbf{d}_1$  and  $\mathbf{d}_3$  ( $\mathbf{d}_2$  and  $\mathbf{d}_4$ ) between the green laser irradiation.

However, in actual experiments,  $\alpha_0^{(k)}$ ,  $\alpha_1^{(k)}$ , and  $\gamma_k$  have a dependency on  $k$  due to inhomogeneities. In this case,

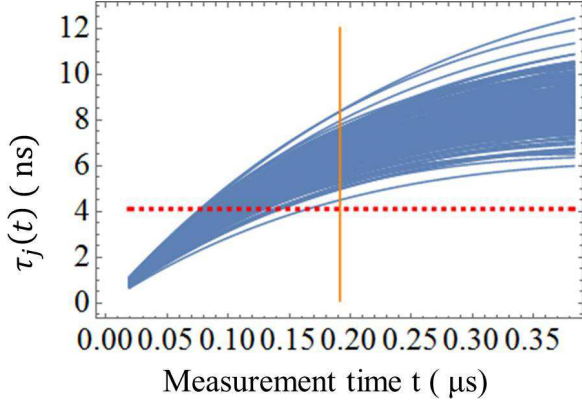


FIG. 4: We plot  $\tau_j(t) = \frac{\alpha_0^{(j)} - \alpha_1^{(j)}}{2} e^{-2\gamma_j t}$  ( $j = 1, 2, \dots, 200$ ) against  $t$  where we choose  $\delta\alpha_j = \alpha_0^{(j)} - \alpha_1^{(j)}$  and  $\gamma_j$  from the Gaussian distribution. The average of  $\delta\alpha_j$  ( $\gamma_j$ ) is 0.01 ( $10^6$  Hz), and the standard deviation is 0.001 ( $10^5$ ). In addition, we plot the value of  $\frac{\delta\alpha_{\min}}{2} e^{-\frac{1}{2} \frac{1}{4\gamma_{\max}}}$  with a horizontal dashed line, where  $\delta\alpha_{\min} = \min_j[\delta\alpha_j]$  and  $\gamma_{\max} = \max_j[\gamma_j]$ , and plot a vertical line at  $t = \frac{1}{4\gamma_{\max}}$ . We numerically show that we can satisfy  $\tau_j(t_j) = \frac{\delta\alpha_{\min}}{2} e^{-\frac{1}{2} \frac{1}{4\gamma_{\max}}}$  for all  $j$  by choosing a certain set of  $\{t_j\}_{j=1}^{200}$  for  $t_j \leq \frac{1}{4\gamma_{\max}}$ .

we need to choose a suitable set of  $t_k$  ( $k = 1, 2, 3, 4$ ) to compensate for such an inhomogeneity. If  $\tau_k(t_k) \equiv \frac{\alpha_0^{(k)} - \alpha_1^{(k)}}{2} e^{-2\gamma_k t_k} t_k$  does not depend on  $k$ , we can measure  $B_x$  from  $\langle \hat{N}_x^{(\text{total})} \rangle$  as described in Eq. (24). We numerically checked that it is possible to have an equal value of  $\frac{\alpha_0^{(k)} - \alpha_1^{(k)}}{2} e^{-2\gamma_k t_k} t_k$  for  $k = 1, 2, 3, 4$ . In Fig. 4, we randomly picked up  $\delta\alpha_k = \alpha_0^{(j)} - \alpha_1^{(j)}$  and  $\gamma_j$  from the Gaussian distribution, and we plotted  $\tau_j(t) = \frac{\alpha_0^{(j)} - \alpha_1^{(j)}}{2} e^{-2\gamma_j t}$  ( $j = 1, 2, \dots, 200$ ). In addition, in the same figure, we plotted the value of  $\frac{\delta\alpha_{\min}}{2} e^{-\frac{1}{2} \frac{1}{4\gamma_{\max}}}$  with a dashed line where  $\delta\alpha_{\min} = \min_j[\delta\alpha_j]$  and  $\gamma_{\max} = \max_j[\gamma_j]$ . These results show that we can choose  $t_j$  to satisfy  $\frac{\alpha_0^{(j)} - \alpha_1^{(j)}}{2} e^{-2\gamma_j t_j} t_j = \frac{\delta\alpha_{\min}}{2} e^{-\frac{1}{2} \frac{1}{4\gamma_{\max}}}$  and  $t_j \leq \frac{1}{4\gamma_{\max}}$  as long as the inhomogeneous width of the parameters is approximately 10% [24]. The expected values of the emitted photons from this state are described as

$$\begin{aligned} \langle \hat{N}_x^{(\text{total})} \rangle &\simeq \sum_{k=1}^4 \frac{\alpha_0^{(k)} + \alpha_1^{(k)}}{2} \\ &- \sum_{k=1,4} \frac{\alpha_0^{(k)} - \alpha_1^{(k)}}{2} g\mu_b \mathbf{B} \cdot \mathbf{d}_k t_k e^{-2\gamma_k t_k} \\ &+ \sum_{k=2,3} \frac{\alpha_0^{(k)} - \alpha_1^{(k)}}{2} g\mu_b \mathbf{B} \cdot \mathbf{d}_k t_k e^{-2\gamma_k t_k} \\ &= \left( \sum_{k=1}^4 \frac{\alpha_0^{(k)} + \alpha_1^{(k)}}{2} \right) + \frac{2e^{-\frac{1}{2}} \delta\alpha_{\min}}{\sqrt{3} 4\gamma_{\max}} g\mu_b B_x \end{aligned}$$

where  $\delta\alpha_{\min} = \min_{k=1,2,3,4}[\alpha_0^{(k)} - \alpha_1^{(k)}]$  and  $\gamma_{\max} = \max_{k=1,2,3,4}[\gamma_k]$ .

Therefore, the uncertainty in the estimation of  $B_x$  is given as follows.

$$\begin{aligned} \delta B_x^{(\text{DC})} &= \frac{\sqrt{\langle \delta \hat{N}_x^{(\text{total})} \delta \hat{N}_x^{(\text{total})} \rangle}}{\left| \frac{d\langle \hat{N}_x^{(\text{total})} \rangle}{dB_x} \right|} \frac{1}{\sqrt{N}} \\ &\simeq \frac{\sqrt{3} \sqrt{\sum_{k=1}^4 \frac{\alpha_0^{(k)} + \alpha_1^{(k)}}{2}}}{2e^{-\frac{1}{2}} \delta\alpha_{\min} g\mu_b \sqrt{\frac{1}{4\gamma_{\max}}}} \frac{1}{\sqrt{T}} \end{aligned} \quad (27)$$

We numerically calculated this sensitivity, and plotted the ratio between the homogeneous case and inhomogeneous case with a standard deviation of  $\sigma$  as shown in Fig. 5. These results demonstrate that, if the standard deviation of the parameters is around a few %, we can achieve nearly the same sensitivity as that in the homogeneous case.

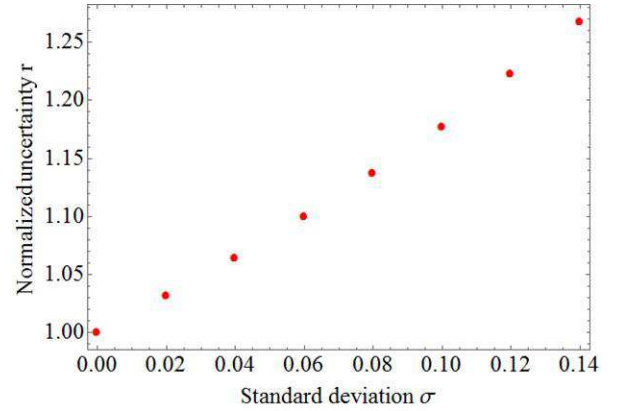


FIG. 5: The normalized uncertainty of the estimation  $r = \delta B_x^{(\text{DC})}(\sigma) / \delta B_x^{(\text{DC})}(\sigma = 0) = \delta B_x^{(\text{AC})}(\sigma) / \delta B_x^{(\text{AC})}(\sigma = 0)$  where  $\delta B_x^{(\text{DC})}(\sigma)$  ( $\delta B_x^{(\text{AC})}(\sigma)$ ) denotes the uncertainty in our DC (AC) vector magnetic field sensor for inhomogeneous parameters with a standard deviation of  $\sigma$ . Note that the normalized uncertainty for the DC sensing has the same form as that for the AC sensing. To calculate the average value, we randomly pick up the values of  $\delta\alpha_j = \alpha_0^{(j)} - \alpha_1^{(j)}$  and  $\gamma_j$  from the Gaussian distribution where the average of  $\delta\alpha_j$  ( $\gamma_j$ ) is  $\overline{\delta\alpha_j} = 0.01$  ( $\overline{\gamma_j} = 10^6$  Hz) and the standard deviation is  $\overline{\delta\alpha_j} \cdot \sigma'$  ( $\overline{\gamma_j} \cdot \sigma'$ ) where  $\sigma'$  denotes a normalized standard deviation.

## AC VECTOR MAGNETIC FIELD SENSOR VIA THE MULTI-FREQUENCY CONTROL

Here, we explain how to measure the AC vector magnetic field using our scheme. As an example, we discuss the case of measuring the x-component of the AC magnetic fields. We use a similar pulse sequence as that in our DC magnetic field sensing. The only difference from the DC magnetic field sensing is that we apply a  $\pi$  pulse in the middle of the microwave

pulse sequence as shown in the Fig. 3 (b). After the green laser irradiation, the state of the photons can be described as follows

$$\rho_{AC}^{(\text{ph})} = \bigotimes_{k=1}^4 \rho_{k,AC}^{(\text{ph})} \quad (28)$$

where

$$\rho_{k,AC}^{(\text{ph})} = \frac{1 + e^{-2\gamma'_k t_k} \sin \theta_k^{(\text{AC})}}{2} \rho_{k,0}^{(\text{ph})} + \frac{1 - e^{-2\gamma'_k t_k} \sin \theta_k^{(\text{AC})}}{2} \rho_{k,1}^{(\text{ph})}$$

for  $k = 2, 3$  and

$$\rho_{k,AC}^{(\text{ph})} = \frac{1 - e^{-2\gamma'_k t_k} \sin \theta_k^{(\text{AC})}}{2} \rho_{k,0}^{(\text{ph})} + \frac{1 + e^{-2\gamma'_k t_k} \sin \theta_k^{(\text{AC})}}{2} \rho_{k,1}^{(\text{ph})}$$

for  $k = 1, 4$ . We can calculate the expected values of the emitted photon from these state as follows

$$\langle \hat{N}_x^{(\text{total})} \rangle \simeq \left( \sum_{k=1}^4 \frac{\alpha_0^{(k)} + \alpha_1^{(k)}}{2} \right) - \sum_{k=1,4} \frac{(\alpha_0^{(k)} - \alpha_1^{(k)}) g \mu_b \mathbf{B} \cdot \mathbf{d}_k \frac{1 + \cos \omega_{AC} t_k - 2 \cos \frac{\omega_{AC} t_k}{2}}{\omega_{AC}} e^{-2\gamma'_k t_k}}{2} + \sum_{k=2,3} \frac{(\alpha_0^{(k)} - \alpha_1^{(k)}) g \mu_b \mathbf{B} \cdot \mathbf{d}_k \frac{1 + \cos \omega_{AC} t_k - 2 \cos \frac{\omega_{AC} t_k}{2}}{\omega_{AC}} e^{-2\gamma'_k t_k}}{2}$$

If we have  $\alpha_0^{(k)} = \alpha_0$ ,  $\alpha_1^{(k)} = \alpha_1$ ,  $\gamma_k = \gamma$ , and  $t_k = t$  for all  $k$ , we obtain

$$\langle \hat{N}_x^{(\text{total})} \rangle \simeq 2(\alpha_0 + \alpha_1) - \frac{2(\alpha_0 - \alpha_1) g \mu_b B_x (1 + \cos \omega_{AC} t - 2 \cos \frac{\omega_{AC} t}{2}) e^{-2\gamma t}}{\sqrt{3} \omega_{AC}} \quad (29)$$

Note that this expectation value only depends on  $B_x$ . Therefore, the uncertainty in the estimation of  $B_x$  is given as follows.

$$\delta B_x^{(\text{AC})} = \frac{\sqrt{\langle \delta \hat{N}_x^{(\text{total})} \delta \hat{N}_x^{(\text{total})} \rangle}}{\left| \frac{d \langle \hat{N}_x^{(\text{total})} \rangle}{dB_x} \right|} \frac{1}{\sqrt{N}} \simeq \frac{\sqrt{2(\alpha_0 + \alpha_1)}}{\frac{2}{\sqrt{3}} |\alpha_0 - \alpha_1| g \mu_b \frac{|1 + \cos \omega_{AC} t - 2 \cos \frac{\omega_{AC} t}{2}|}{\omega_{AC}} e^{-2\gamma t}} \frac{1}{\sqrt{\frac{T}{t}}} \quad (30)$$

where  $N = \frac{T}{t}$  denotes the repetition number of the experiment. By optimizing the parameters, we obtain

$$\delta B_x^{(\text{AC})} \simeq \frac{\sqrt{3} \sqrt{2(\alpha_0 + \alpha_1)}}{2e^{-\frac{1}{2}} |\alpha_0 - \alpha_1| g \mu_b \frac{|1 + \cos \theta_{\text{opt}} - 2 \cos \frac{\theta_{\text{opt}}}{2}|}{\theta_{\text{opt}}}} \frac{1}{\sqrt{\frac{1}{4\gamma'}}} \sqrt{T}$$

Because  $\alpha_0 \simeq \alpha_1$ , we can conclude that the sensitivity of our scheme is approximately four times better than that in the conventional scheme by comparing Eq. (31) with the Eq. (17).

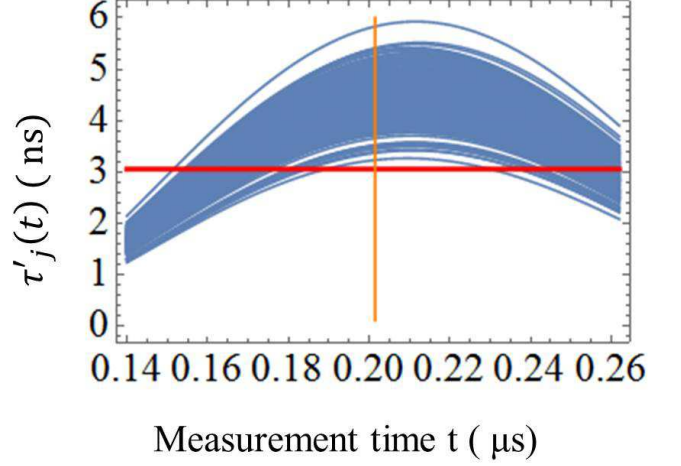


FIG. 6: We plot  $\tau'_j(t) = \frac{\alpha_0^{(j)} - \alpha_1^{(j)}}{2} e^{-2\gamma'_j t} \frac{1 + \cos(\omega_{AC} t) - 2 \cos(\frac{\omega_{AC} t}{2})}{\omega_{AC}}$  ( $j = 1, 2, \dots, 200$ ) against  $t$  where we choose  $\delta\alpha_j = \alpha_0^{(j)} - \alpha_1^{(j)}$  and  $\gamma'_j$  from the Gaussian distribution. The average of  $\delta\alpha_j$  ( $\gamma'_j$ ) is  $0.01$  ( $10^6$ ), and the standard deviation is  $0.001$  ( $10^5$ ). In addition, we plot the value of  $\frac{\delta\alpha_{\min}}{2} e^{-\frac{1}{2}} \frac{1 + \cos(\theta_{\text{opt}}) - 2 \cos(\frac{\theta_{\text{opt}}}{2})}{\omega_{AC}}$  with a horizontal dashed line, and we plot a vertical line at  $t = \frac{1}{4\gamma'_{\max}}$  where  $\delta\alpha_{\min} = \min_k[\delta\alpha_j]$ ,  $\gamma'_{\max} = \max_j[\gamma'_j]$ , and  $\omega_{AC} = 4\theta_{\text{opt}}\gamma'_{\max}$ . We numerically show that we can satisfy  $\tau'_j(t_j) = \frac{\delta\alpha_{\min}}{2} e^{-\frac{1}{2}} \frac{1 + \cos(\theta_{\text{opt}}) - 2 \cos(\frac{\theta_{\text{opt}}}{2})}{\omega_{AC}}$  for all  $j$  by choosing a certain set of  $\{t_j\}_{j=1}^{200}$  where  $t_j \leq \frac{1}{4\gamma'_{\max}}$ .

Conversely, if the parameters  $\alpha_0^{(k)}$ ,  $\alpha_1^{(k)}$ , and  $\gamma'_k$  have a dependency on  $k$ , we need to choose a suitable set of  $t_k$  ( $k = 1, 2, 3, 4$ ) to compensate such an inhomogeneity. We know that, if  $(\alpha_0^{(k)} - \alpha_1^{(k)}) e^{-2\gamma'_k t_k} \frac{1 + \cos \omega_{AC} t_k - 2 \cos \frac{\omega_{AC} t_k}{2}}{\omega_{AC}}$  does not depend on  $k$ , we can estimate the value of  $B_x$  from just  $\langle \hat{N}_x^{(\text{total})} \rangle$ . We numerically checked if it is possible to have an equal value of  $(\alpha_0^{(k)} - \alpha_1^{(k)}) e^{-2\gamma'_k t_k} \frac{1 + \cos \omega_{AC} t_k - 2 \cos \frac{\omega_{AC} t_k}{2}}{\omega_{AC}}$ . In Fig. 6, we randomly picked  $\delta\alpha_j = \alpha_0^{(j)} - \alpha_1^{(j)}$  and  $\gamma'_j$  from the Gaussian distribution. We plotted  $\tau'_j(t) = \frac{\alpha_0^{(j)} - \alpha_1^{(j)}}{2} e^{-2\gamma'_j t} \frac{1 + \cos(\omega_{AC} t) - 2 \cos(\frac{\omega_{AC} t}{2})}{\omega_{AC}}$  ( $j = 1, 2, \dots, 200$ ) and the value of  $\frac{\delta\alpha_{\min}}{2} e^{-\frac{1}{2}} \frac{1 + \cos(\theta_{\text{opt}}) - 2 \cos(\frac{\theta_{\text{opt}}}{2})}{\omega_{AC}}$  where  $\delta\alpha_{\min} = \min_j[\delta\alpha_j]$ ,  $\gamma'_{\max} = \max_j[\gamma'_j]$ , and  $\omega_{AC} = 4\theta_{\text{opt}}\gamma'_{\max}$ . These results show that we can choose  $t_j$  to satisfy  $\tau'_j(t_j) = \frac{\delta\alpha_{\min}}{2} e^{-\frac{1}{2}} \frac{1 + \cos(\theta_{\text{opt}}) - 2 \cos(\frac{\theta_{\text{opt}}}{2})}{\omega_{AC}}$  for all  $j$  where  $t_j \leq \frac{1}{4\gamma'_{\max}}$ .

We can calculate the expected values of the emitted photons

from this state as follows:

$$\begin{aligned} & \langle \hat{N}_x^{(\text{total})} \rangle \\ & \simeq \left( \sum_{k=1}^4 \frac{\alpha_0^{(k)} + \alpha_1^{(k)}}{2} \right) \\ & - \frac{2e^{-\frac{1}{2}} \delta\alpha_{\min} g \mu_b B_x (1 + \cos\theta_{\text{opt}} - 2 \cos\frac{\theta_{\text{opt}}}{2})}{\sqrt{3}\omega_{\text{AC}}} \end{aligned} \quad (31)$$

where  $\delta\alpha_{\min} = \min_{k=1,2,3,4}[\delta\alpha_k]$ ,  $\gamma'_{\max} = \max_{k=1,2,3,4}[\gamma'_k]$ , and  $\omega_{\text{AC}} = 4\theta_{\text{opt}}\gamma'_{\max}$ . Therefore, the uncertainty is

$$\delta B_x^{(\text{AC})} \simeq \frac{\sqrt{3} \sqrt{\sum_{k=1}^4 \frac{\alpha_0^{(k)} + \alpha_1^{(k)}}{2}}}{2e^{-\frac{1}{2}} \delta\alpha_{\min} g \mu_b \frac{|1 + \cos\theta_{\text{opt}} - 2 \cos\frac{\theta_{\text{opt}}}{2}|}{\theta_{\text{opt}}}} \frac{1}{\sqrt{4\gamma'_{\max}}} \frac{1}{\sqrt{T}} \quad (32)$$

Similar to the case of DC vector magnetic field sensing, we can achieve nearly the same sensitivity as that in the homogeneous case if the standard deviation of the parameters is around a few % as shown in Fig. 5.

In conclusion, we proposed a scheme to improve the sensitivity of the vector magnetic field sensing via multi-frequency control. Implementing a Ramsey interference or spin echo experiment for all NV centers with different NV axes using frequency selectivity, we can enhance the signal from the NV centers. We demonstrated that the sensitivity of the vector magnetic field sensing becomes approximately four times better than that of the conventional scheme.

We thank Suguru Endo for useful discussion. This work was supported by JSPS KAKENHI Grant No. 15K17732. This work was also supported by MEXT KAKENHI Grants No. 15H05868, No. 15H05870, No. 15H03996, No. 26220602 and No. 26249108. This work was also supported by Advanced Photon Science Alliance (APSA), JSPS core-to-core Program and Spin-NRJ.

---

[1] J. Simon, *Advances in Physics* **48**, 449 (1999).  
[2] A. Chang, H. Hallen, L. Harriott, H. Hess, H. Kao, J. Kwo, R. Miller, R. Wolfe, J. Van der Ziel, and T. Chang, *Appl. Phys. Lett.* **61**, 1974 (1992).  
[3] M. Poggio and C. Degen, *Nanotechnology* **21**, 342001 (2010).  
[4] J. Maze, P. Stanwix, J. Hodges, S. Hong, J. Taylor, P. Cappellaro, L. Jiang, M. Dutt, E. Togan, A. Zibrov, et al., *Nature* **455**, 644 (2008), ISSN 0028-0836.  
[5] J. Taylor, P. Cappellaro, L. Childress, L. Jiang, D. Budker, P. Hemmer, A. Yacoby, R. Walsworth, and M. Lukin, *Nature Physics* **4**, 810 (2008).

[6] G. Balasubramanian, I. Chan, R. Kolesov, M. Al-Hmoud, J. Tisler, C. Shin, C. Kim, A. Wojcik, P. Hemmer, A. Krueger, et al., *Nature* **455**, 648 (2008).  
[7] M. Schaffry, E. Gauger, J. Morton, and S. Benjamin, *Phys. Rev. Lett.* **107**, 207210 (2011).  
[8] G. Davies, *Properties and Growth of Diamond* (Inspec/lee, 1994).  
[9] A. Gruber, A. Dräbenstedt, C. Tietz, L. Fleury, J. Wrachtrup, and C. Von Borczyskowski, *Science* **276**, 2012 (1997).  
[10] F. Jelezko, I. Popa, A. Gruber, C. Tietz, J. Wrachtrup, A. Nizovtsev, and S. Kilin, *Appl. Phys. Lett.* **81**, 2160 (2002).  
[11] F. Jelezko, T. Gaebel, I. Popa, A. Gruber, and J. Wrachtrup, *Phys. Rev. Lett* **92**, 076401 (2004).  
[12] G. Balasubramanian, P. Neumann, D. Twitchen, M. Markham, R. Kolesov, N. Mizuochi, J. Isoya, J. Achard, J. Beck, J. Tisler, et al., *Nature materials* **8**, 383 (2009).  
[13] N. Mizuochi, P. Neumann, F. Rempp, J. Beck, V. Jacques, P. Siyushev, K. Nakamura, D. Twitchen, H. Watanabe, S. Yamasaki, et al., *Physical review B* **80**, 041201 (2009).  
[14] N. Bar-Gill, L. M. Pham, A. Jarmola, D. Budker, and R. L. Walsworth, *Nature communications* **4**, 1743 (2013).  
[15] R. Schirhagl, K. Chang, M. Loretz, and C. L. Degen, *Annual review of physical chemistry* **65**, 83 (2014).  
[16] B. Maertz, A. Wijnheijmer, G. Fuchs, M. Nowakowski, and D. Awschalom, *Applied Physics Letters* **96**, 092504 (2010).  
[17] S. Steinert, F. Dolde, P. Neumann, A. Aird, B. Naydenov, G. Balasubramanian, F. Jelezko, and J. Wrachtrup, *Review of scientific instruments* **81**, 043705 (2010).  
[18] L. M. Pham, D. Le Sage, P. L. Stanwix, T. K. Yeung, D. Glenn, A. Trifonov, P. Cappellaro, P. Hemmer, M. D. Lukin, H. Park, et al., *New Journal of Physics* **13**, 045021 (2011).  
[19] J. Tetienne, L. Rondin, P. Spinicelli, M. Chipaux, T. Debuisschert, J. Roch, and V. Jacques, *New Journal of Physics* **14**, 103033 (2012).  
[20] A. K. Dmitriev and A. K. Vershovskii, *JOSA B* **33**, B1 (2016).  
[21] K. Sasaki, Y. Monnai, S. Saijo, R. Fujita, H. Watanabe, J. Ishihayase, K. M. Itoh, and E. Abe, *Review of Scientific Instruments* **87**, 053904 (2016).  
[22] D. Le Sage, K. Arai, D. Glenn, S. DeVience, L. Pham, L. Rahn-Lee, M. Lukin, A. Yacoby, A. Komeili, and R. Walsworth, *Nature* **496**, 486 (2013).  
[23] A. Nowodzinski, M. Chipaux, L. Toraille, V. Jacques, J.-F. Roch, and T. Debuisschert, *Microelectronics Reliability* **55**, 1549 (2015).  
[24] V. Acosta, E. Bauch, M. Ledbetter, C. Santori, K.-M. Fu, P. Barclay, R. Beausoleil, H. Linget, J. Roch, F. Treussart, et al., *Physical Review B* **80**, 115202 (2009).  
[25] J. Michl, T. Teraji, S. Zaiser, I. Jakobi, G. Waldherr, F. Dolde, P. Neumann, M. W. Doherty, N. B. Manson, J. Isoya, et al., *Applied Physics Letters* **104**, 102407 (2014).  
[26] M. Lesik, J.-P. Tetienne, A. Tallaire, J. Achard, V. Mille, A. Gicquel, J.-F. Roch, and V. Jacques, *Applied Physics Letters* **104**, 113107 (2014).  
[27] T. Fukui, Y. Doi, T. Miyazaki, Y. Miyamoto, H. Kato, T. Matsumoto, T. Makino, S. Yamasaki, R. Morimoto, N. Tokuda, et al., *Applied Physics Express* **7**, 055201 (2014).